arXiv:1701.04564v1 [math.NA] 17 Jan 2017

A numerical study of branching and stability of solutions to three-dimensional martensitic phase transformations using gradient-regularized, non-convex, finite strain elasticity

K. Sagiyama*, S. Rudraraju† and K. Garikipati‡

January 18, 2017

Abstract

In the setting of continuum elasticity, phase transformations involving martensitic variants are modeled by a free energy density function that is non-convex in strain space. Here, we adopt an existing mathematical model in which we regularize the non-convex free energy density function by higher-order gradient terms at finite strain and derive boundary value problems via the standard variational argument applied to the corresponding total free energy, inspired by Toupin's theory of gradient elasticity. These gradient terms are to preclude existence of arbitrarily fine microstructures, while still allowing for existence of multiple solution branches corresponding to local minima of the total free energy; these are classified as *metastable* solution branches. The goal of this work is to solve the boundary value problem numerically in three dimensions, observe solution branches, and assess stability of each branch by numerically evaluating the second variation of the total free energy. We also study how these microstructures evolve as the length-scale parameter, the coefficient of the strain gradient terms in the free energy, approaches zero.

keywords— phase-transformation, twinning, three-phase equilibrium, meta-stability, non-convex free energy.

1 Introduction

Many multi-component solids, such as shape memory alloys (NiTi), involve phase transformations from cubic austenite to tetragonal martensite crystal structures. The tetragonal lattice is characterized by transformation strains relative to the undistorted reference cubic structure. The strain splits the symmetry group of the cubic lattice into three equivalent sub-groups, each of which corresponds to a tetragonal lattice oriented along one of the cubic crystal axes. These tetragonal variants accommodate themselves in a body to achieve configurations that are local energy minimizers while maintaining kinematic compatibility. As a result, *twin* microstructures form with a tiled appearance due to the near constancy of strain within each twinned sub-domain.

The underlying phenomenology can be described by a free energy density function that is non-convex in a frame-invariant strain measure, to account for the finite deformation, and admits three minima corresponding to the tetragonal variants. The classical variational treatment of elasticity only identifies stationary points, while of particular interest are the *metastable* solution branches that correspond to local minima of the total energy. These metastable branches are to be identified in this work by examining the stability of solutions obtained by numerically solving the boundary value problems arising from the variational formulation.

Configurations that minimize the total free energy on a given domain with boundaries have been studied in the setting of sharp-interface models by constructing sequences that converge weakly to the minimizer [1, 3]. Although this approach provides one with good insights to various classes of problems, it allows for arbitrarily fine twin microstructures—a non-physical aspect of the mathematical formulation resulting from the absence of interface energies associated with the martensitic phase boundaries. Diffuse-interface models resolve this pathology by including higher-order, strain gradient-dependent terms representing the interfacial energy; the coefficients of the higher-order gradient terms, which control the twin interface thicknesses, give rise to *length-scale parameters*. As diffuse-interface models directly taking into account the total free energy, they also make it straightforward to solve general boundary value problems, provided that the high-order gradients in the partial differential equation can be suitably treated, to solve problems that involve energy wells of unequal

*Mechanical Engineering, University of Michigan
†Mechanical Engineering, University of Michigan
‡Mechanical Engineering and Mathematics, University of Michigan, corresponding author krishna@umich.edu

depths, and to investigate stability/metastability of solution branches via investigation of the second variation of the total energy. One-dimensional models have been intensively studied in this context: Carr et al. [2] showed, for standard one-dimensional problems with Dirichlet and higher-order Neumann boundary conditions, that mere inclusion of the higher-order strain gradient energy terms only leaves a pair of stable solutions, the global minimizers of the total energy, which have only a single *phase boundary*. These solutions, however, do not represent experimentally obtained microstructures that have twin layers separated by multiple phase boundaries. This gap in the representation was resolved by Truskinovsky and Zanzotto [12, 13] and by Vainchtein and co-workers [14, 15] by adding to the model an elastic support that represents the multi-dimensional effect. This allowed the successful recovery of metastable solution branches corresponding to local minimizers of the total energy. Healey and Miller [5] studied an anti-plane shear model of martensite-martensite phase transformations for pure Dirichlet problems in two dimensions, and obtained metastable solution branches over a range of values of the length scale parameter. Numerical work in this field has included *branch-tracking* techniques to obtain metastable solution branches and evaluation of the second variation of the total free energy to assess their stability [14, 15, 5].

While one-dimensional problems and some restricted, linearized two-dimensional problems may be partially aided by analysis, the complete, nonlinear, three-dimensional treatment at finite strain with general boundary conditions must be numerical. Rudraraju et al. [7] have adopted spline-based (isogeometric analytic) numerical methods to obtain three-dimensional solutions to general boundary value problems of Toupin's theory of gradient elasticity at finite strain [9]. This approach makes it possible to study a wide diversity of problems. In this communication we present numerical solutions to diffuse-interface problems of phase transformations between martensitic variants under traction loading in three dimensions. The fundamental framework to study metastable branches is the same as that used previously in the literature [14, 15, 5]. We obtain numerical solutions to boundary value problems from a starting guess. Particular solution branches are tracked as the strain gradient length scale parameter is varied, and stability of a given branch is determined by numerically examining the second variation of the total free energy. To the best of our knowledge, this is the first three-dimensional study of twin microstructures and their stability using gradient-regularized non-convex elasticity. Of further note is that we apply arbitrary boundary conditions. Crucial to our work is the numerical framework derived from the work of Rudraraju et al. [7].

In Sec. 2 we present an overview of the fundamental ideas using a simple problem in one dimension. Three-dimensional problems are then studied in Sec. 3 employing virtually the same numerical techniques. Conclusions and future studies are discussed in Sec. 4.

2 A one-dimensional primer

Branching in three dimensions being our eventual concern, it is instructive to first study a related problem in one dimension.

The one-dimensional free energy density, $\Psi_{1\mathrm{D}}$, is defined as a function of strain and strain-gradient derived from the solution field $u(X)$ as:

$$\Psi_{1\mathrm{D}} = (u_{,X}^4 - 2u_{,X}^2) + l^2 u_{,XX}^2, \tag{1}$$

where l is the strain gradient length-scale parameter. This energy density (1) is non-convex with respect to the strain component $u_{,X}$; see Fig. 1a. In the absence of the strain-gradient contribution; i.e., with $l = 0$ in (1), this non-convex density function characterizes fields u that are composed purely of two variants, one with $u_{,X} = -1$ and the other with $u_{,X} = +1$; see Fig. 1b. In this setting laminae (sub-domains) of these two variants form with arbitrary size, and in principle, infinitely fine microstructures can develop. The length scale parameter l precludes the existence of such twinned microstructures of infinite fineness by penalizing the interfaces between them. It also introduces a characteristic length scale to the problem.

We seek solution fields $u \in \mathcal{S}_{1D}$ on $\overline{\Omega}_{1D}$, where $\Omega_{1D} = (0, 1)$, that satisfy standard and higher-order Dirichlet boundary conditions:

$$u = 0,\ u_{,X} = 0 \quad \text{on } X = 0, \tag{2a}$$

$$u = d,\ u_{,X} = 0 \quad \text{on } X = 1, \tag{2b}$$

where $d = 2^{-10}$, and globally/locally minimize the total free energy corresponding to the density function (1):

$$\Pi_{1\mathrm{D}} := \int_{\Omega_{1\mathrm{D}}} \Psi_{1\mathrm{D}}\ \mathrm{d}\Omega_{1\mathrm{D}}. \tag{3}$$

To this end, we define admissible test functions $w \in \mathcal{V}_{1D}$ that satisfy:

$$w = 0,\ w_{,X} = 0 \quad \text{on } X = 0, \tag{4a}$$

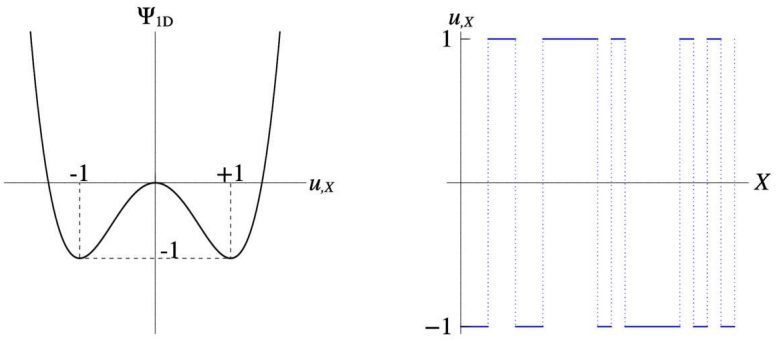

(a) (b)

Figure 1: Plots of (a) free energy density function Ψ_{1D} projected onto the Ψ_{1D}–$u_{,X}$ plane and (b) a typical solution that minimizes the total free energy when $l = 0$ in (1).

$$w = 0,\ w_{,X} = 0 \quad \text{on } X = 1, \tag{4b}$$

and solve the following weak form of the boundary value problem derived from the variational argument: Find $u \in \mathcal{S}_{1D}$ such that $\forall w \in \mathcal{V}_{1D}$,

$$D\Pi_{1D}[w] = \int_{\Omega_{1D}} (w_{,X} P + w_{,XX} B)\ \mathrm{d}\Omega_{1D} = 0, \tag{5}$$

where P is the first Piola-Kirchhoff stress and B is the higher-order stress, defined as:

$$P := \partial\Psi_{1D}/\partial u_{,X}, \tag{6a}$$
$$B := \partial\Psi_{1D}/\partial u_{,XX}. \tag{6b}$$

Stability of the solutions is then assessed by examining the positive definiteness of the second variation:

$$D^2\Pi_{1D}[w, w] = \int_{\Omega_{1D}} \left(w_{,X} \frac{\partial^2\Psi_{1D}}{\partial u_{,X}\partial u_{,X}} w_{,X} + w_{,X} \frac{\partial^2\Psi_{1D}}{\partial u_{,X}\partial u_{,XX}} w_{,XX} + w_{,XX} \frac{\partial^2\Psi_{1D}}{\partial u_{,XX}\partial u_{,X}} w_{,X} + w_{,XX} \frac{\partial^2\Psi_{1D}}{\partial u_{,XX}\partial u_{,XX}} w_{,XX} \right) \mathrm{d}\Omega_{1D} > 0, \tag{7}$$

where we have explicitly retained the symmetric second and third terms of the integrand for clarity of the development. Note that weak form (5) and (2) with (4) leads us to the following strong form:

$$-P_{,X} + B_{,XX} = 0 \quad \text{on } \Omega_{1D},$$

which possesses fourth-order spatial derivatives due to the constitutive relations (1), (6a) and (6b). This strong form is not investigated further in this work.

2.1 The numerical framework

We seek numerical solutions $u^h \in \mathcal{S}^h_{1D} \subset \mathcal{S}_{1D}$ to a discretized counterpart of the weak from (5) with the test functions $w^h \in \mathcal{V}^h_{1D} \subset \mathcal{V}_{1D}$ where:

$$\mathcal{S}^h_{1D} = \{v^h \in H^2(\Omega_{1D}) | v^h = 0,\ v^h_{,X} = 0 \text{ on } X = 0,\ v^h = d,\ v^h_{,X} = 0 \text{ on } X = 1\}, \tag{8a}$$
$$\mathcal{V}^h_{1D} = \{v^h \in H^2(\Omega_{1D}) | v^h = 0,\ v^h_{,X} = 0 \text{ on } X = \{0, 1\}\}, \tag{8b}$$

where H^2 represents the standard Sobolev space of integrable functions with integrable first and second derivatives. The problem was solved using isogeometric analysis (IGA) with fourth-order B-spline basis functions defined on 1024 elements of uniform size on Ω_{1D}; see Cottrell et al. [4] for a comprehensive treatment of IGA, and Rudraraju et al. [7] for its application to the current problem framework, but with weak enforcement of Dirichlet boundary conditions. We use the quartic-precision floating-point format and solve for solutions up to

an absolute tolerance of 10^{-25} in the Euclidean norm of the residual corresponding to the discretized version of (5). The higher than typical precision and more stringent tolerance are important to verify convergence to extrema/saddle points of the rapidly fluctuating free energy functional that governs this problem. This rapid fluctuation underlies the existence of families of stable/unstable solutions, which is the crux of this work. The second variation in (7) is discretized on the same B-spline basis, and stability is assessed by examining the positive definiteness of the resulting symmetric Hessian matrix using the eigenvalue solver FEAST v3.0 [6] with the relative accuracy of $O(10^{-8})$. Figures were produced using mathgl 2.3.0.

2.2 Solution branches and branch-tracking

Fig. 2a shows the total free energy, $\Pi_{1\mathrm{D}}$, of solutions to the boundary value problem, plotted against the length scale parameter l, where six representative branches are labeled as A - F. Numerically computed strains, $u_{,X}$, are plotted against X in Fig. 3 for branches A-F at selected values of l.

Here, we outline the procedure that we used to obtain the branches shown in Fig. 2a. In solving the nonlinear boundary value problem (5) and (2) with (4), we observed that the homogeneous initial guess $u_{\mathrm{init}} = 0$ always captures the branch of highest energy at each l as seen in Fig. 2, where these solutions are represented by green squares; discontinuities present in the sequence of green squares are good indicators of the existence of multiple brunches. The blue solid lines in Fig. 2, on the other hand, are obtained by a simple *branch-tracking* technique. We first chose a starting value of l and an initial guess for the solution u_{init}, and solved the problem for $\bar{u}(l)$. We then incremented/decremented l by a small amount Δl and solved this updated problem for $\bar{u}(l+\Delta l)$ using $\bar{u}(l)$ as the initial guess. We repeated this process of using the previous solution as the initial guess for the updated problem to extend the smooth energy curves shown in Fig. 2. This method helped us to *stay* on the branch that the very first solution happened to fall onto. In our numerical experiments the first solutions were obtained in two different ways: using the homogeneous initial guess and using random initial guesses. Specifically, branches B, D, and F were first solved using the homogeneous initial guess at $l = 0.20$, $l = 0.10$, and $l = 0.08$, followed by incrementation/decrementation of l. Branches B, D, and F obtained in this way respect *geometric symmetry* (cf. [13]) of the boundary value problem at least for large enough l; contrary to the case considered in Sec. 3.4 of [13], elastic supports are absent in our problem and one can see that the translated solution fields $\tilde{u}(X) := u(X) - d/2$ of these branches satisfy $\tilde{u}(X) = -\tilde{u}(1-X)$, and thus $\tilde{u}_{,X}(X) = \tilde{u}_{,X}(1-X)$. Branches A, C, and E, on the other hand, are asymmetric. Those branches were obtained using random initial guesses at $l = 0.10$, $l = 0.10$, and $l = 0.05$, and then branch-tracking.

2.3 Stability

We performed a numerical stability analysis by evaluating the positive definiteness of the Hessians corresponding to the second variation (7) of the continuous problem for branches A - F, of increasing total free energy. We recall that if we find multiple solution branches corresponding to local minima of the total free energy, these are classified as *metastable*. Our analysis showed that the lowest branch, A, is stable up to $l = 0.225$, at which value it meets branch B in the $\Pi_{1\mathrm{D}} - l$ space, branch B is stable for $l > 0.225$, and there exists no metastable solution branch at any l; see Figs. 2a and 2b. In [2] it was shown that, if higher-order Neumann boundary conditions $u_{,XX} = 0$ are applied at both ends instead of the higher-order Dirichlet conditions $u_{,X} = 0$ as in (2), the only stable branch is the one of lowest energy and no metastable branch exists for the type of energy density defined in (1). Although the boundary conditions employed here are different, leading to the particular $\Pi_{1\mathrm{D}} - l$ free energy landscapes in Fig. 2a, our observation is essentially consistent with the analysis given in [2].

3 Branching and stability of solutions in three-dimensional, non-convex elasticity

We now turn our attention to the main focus of this communication: branching in three-dimensional problems. In related two dimensional work [5] the branching of solutions was studied for two-phase elastic solids with pure Dirichlet boundaries using a non-convex free energy density function also regularized by strain-gradient terms. There, the associated Euler-Lagrange equation admitted the trivial solution, allowing for a local bifurcation analysis. The equations were first linearized to find *bifurcation points*, i.e. values of the length-scale parameter at which solution branches bifurcate from the trivial solution. The local bifurcation analysis was then followed by a global bifurcation analysis, where solution branches were continued along the length-scale parameter from those bifurcation points, solving the original nonlinear equation using a branch-tracking technique. The stability of those branches was then assessed by numerically checking the positive definiteness of the second variation of the total free energy. The same technique was also used by Vainchtein and co-workers [15] for one-dimensional problems.

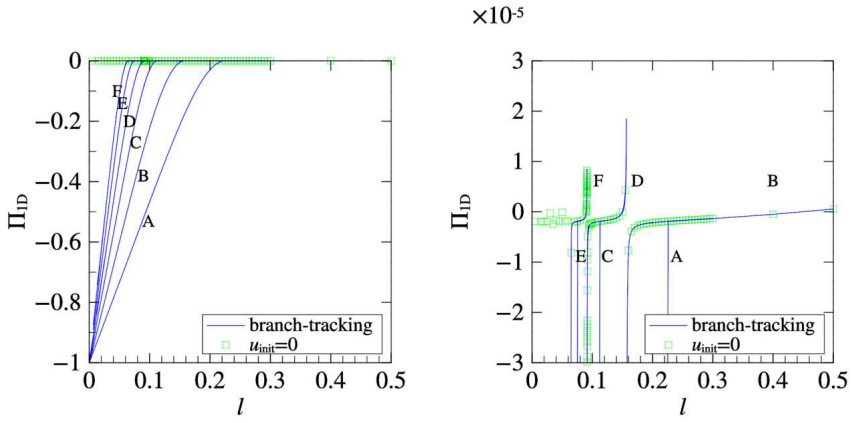

(a) (b)

Figure 2: Plots of total free energy Π_{1D} v.s. length scale parameter l on (a) $(l, \Pi_{1D}) \in [0, 0.5] \times [-1, 3 \times 10^{-5}]$ and (b) $(l, \Pi_{1D}) \in [0, 0.5] \times [-3 \times 10^{-5}, 3 \times 10^{-5}]$ for selected branches. Green squares were computed using the homogeneous initial guess, $u_{\text{init}} = 0$, while blue solid curves were obtained by branch-tracking. Branches A - F are labeled.

Here, we carry out a numerical, three-dimensional study of an elastic solid that undergoes phase transformations between three tetragonal variants under traction loads to form branches. We chose to work on a body subject to traction because one of our ultimate goals is the simulation of shape-memory alloys, where such traction boundary conditions naturally arise. For the boundary value problem governed by non-convex elasticity, regularized by Toupin's theory of gradient elasticity at finite strain, only pure numerical approaches are feasible to compute branches, using the methods described in Sec. 2, instead of the ones based on local bifurcation analysis. The stability of each solution is assessed as described in Sec. 2 using the second variation of the total free energy.

The non-dimensionalized free-energy density function is defined in terms of gradients and strain gradients of the displacement field $\boldsymbol{u}(\boldsymbol{X})$ as:

$$\begin{aligned}\Psi := {} & B_1 e_1^2 + B_2(e_2^2 + e_3^2) + B_3 e_3(e_3^2 - 3e_2^2) + B_4(e_2^2 + e_3^2)^2 + B_5(e_4^2 + e_5^2 + e_6^2) \\ & + l^2(e_{2,1}^2 + e_{2,2}^2 + e_{2,3}^2 + e_{3,1}^2 + e_{3,2}^2 + e_{3,3}^2),\end{aligned} \tag{9}$$

where $B_1, ..., B_5$ are constants and the following reparameterized strain measures were used:

$$e_1 = \frac{E_{11} + E_{22} + E_{33}}{\sqrt{3}}, \qquad e_2 = \frac{E_{11} - E_{22}}{\sqrt{2}}, \qquad e_3 = \frac{E_{11} + E_{22} - 2E_{33}}{\sqrt{6}} \tag{10a}$$

$$e_4 = E_{23} = E_{32}, \qquad e_5 = E_{13} = E_{31}, \qquad e_6 = E_{12} = E_{21}, \tag{10b}$$

where $E_{IJ} = 1/2(F_{kI}F_{kJ} - \delta_{IJ})$ are components of the Green-Lagrange strain tensor, $F_{iJ} = \delta_{iJ} + u_{i,J}$ being components of the deformation gradient tensor. Here as elsewhere $(\cdot)_{,J}$ denotes spatial derivatives with respect to the reference rectangular Cartesian coordinate variable X_J $(J = 1, 2, 3)$. Throughout this work we set $B_5 = 180$, $B_1 = 3.25B_5$, $B_2 = -1.5/r^2$, $B_3 = 1.0/r^3$, and $B_4 = 1.5/r^4$, where $r = 0.25$, unless otherwise noted. At $e_2, e_3 = 0$, corresponding to deformations that reduce to volumetric dilatations in the infinitesimal strain limit, the free energy density function (9) possesses a local maximum in $e_2 - e_3$ space and represents the cubic austenite crystal structure. The reference, unstrained state is also in the cubic austenite structure. Thus defined, Ψ is non-convex with respect to the strain variables e_2 and e_3 and possesses three minima, or *energy wells*, of unit depth located at a distance of 0.25 from the origin on the $e_2 - e_3$ plane; see Fig. 4a. These three energy wells represent three martensitic variants of symmetrically equivalent tetragonal crystal structures, elongated in the X_1-, X_2-, and X_3-directions, respectively, that are colored/numbered in Fig. 4a. As an example, a characteristic configuration that achieves minimum energy density of -1 almost everywhere for $l = 0$ in (9) appears in Fig. 4b, showing laminae of variant 1 and variant 2. In our numerical example a tetragonal variant is regarded as present at a point of the body if the energy density on this $e_2 - e_3$ plane is less than -0.5 at that point.

We are interested in solution fields $\boldsymbol{u}(\boldsymbol{X})$ on a unit cube $\overline{\Omega}$, where $\Omega = (0, 1)^3$, that satisfy the following Dirichlet boundary conditions:

$$u_i = 0, \; u_{i,1} = 0 \quad \text{on } X_1 = 0, \quad i = 1, 2, 3, \tag{11a}$$

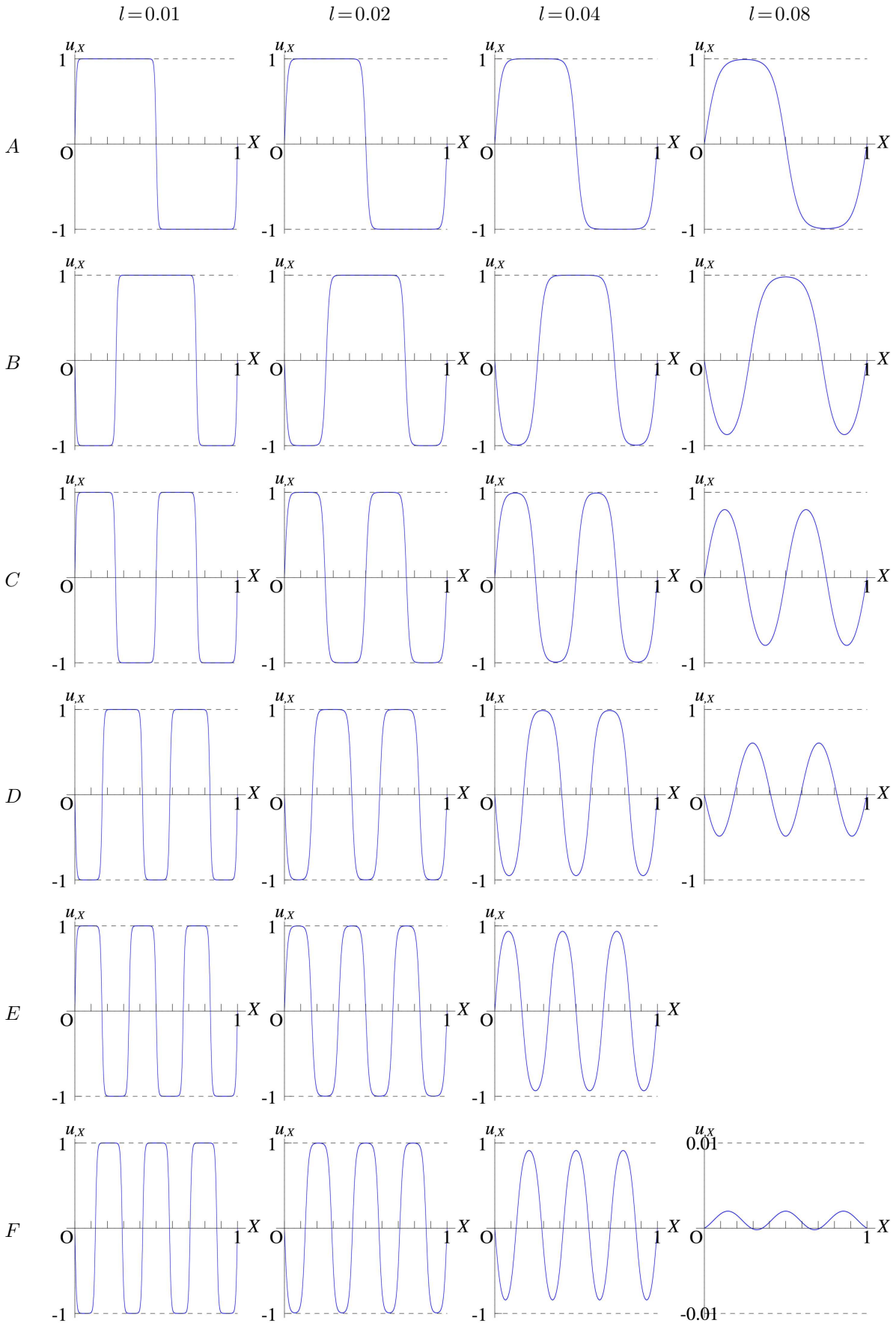

Figure 3: Plots of computed strain $u_{,X}$ for branches A - F at selected values of l.

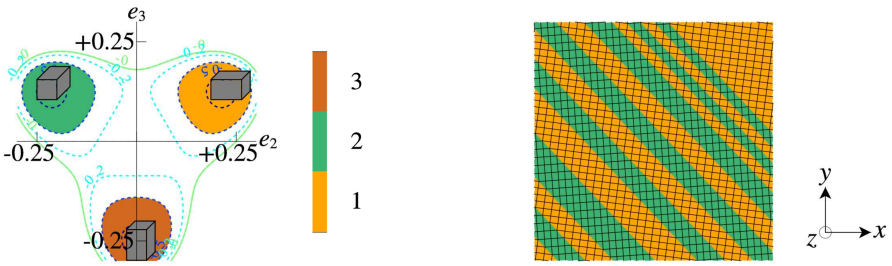

(a) (b)

Figure 4: (a) Contour plots of Ψ projected onto the $e_2 - e_3$ plane; contour curves of $\Psi = 0, -0.2, -0.5, -0.9$ are shown. Three tetragonal variants are colored/numbered. A tetragonal variant is regarded as present at a point of the body if the energy density on this $e_2 - e_3$ plane is less than -0.5 at that point. (b) A two-dimensional slice of a typical microstructure in three dimensions that minimizes the total free energy when $l = 0$ in (9). Twinning is formed between Variants 1 and 2.

$$u_1 = 0,\ u_{1,1} = 0 \quad \text{on } X_1 = 1, \tag{11b}$$

and globally/locally minimize the total free energy corresponding to the density function (9):

$$\Pi := \int_\Omega \Psi \, \mathrm{d}\Omega - \int_{\Gamma_{X_1=1}} (u_2 T_2 + u_3 T_3) \, \mathrm{d}\Gamma_{X_1=1}, \tag{12}$$

where $T_2 = T_3 = 0.01$ are the standard tractions on the reference boundary $X_1 = 1$ denoted by $\Gamma_{X_1=1}$. The standard traction vanishes on the boundaries $X_2 = \{0, 1\}$, $X_3 = \{0, 1\}$, and higher-order tractions vanish wherever higher-order Dirichlet conditions are not prescribed [9, 10]. We define admissible test functions $\boldsymbol{w} \in \mathcal{V}$ that satisfy:

$$w_i = 0,\ w_{i,1} = 0 \quad \text{on } X_1 = 0, \quad i = 1, 2, 3, \tag{13a}$$
$$w_1 = 0,\ w_{1,1} = 0 \quad \text{on } X_1 = 1, \tag{13b}$$

and solve the following weak form of the boundary value problem derived from variational arguments [9, 10, 7]:

$$D\Pi[\boldsymbol{w}] = \int_\Omega (w_{i,J} P_{iJ} + w_{i,JK} B_{iJK}) \, \mathrm{d}\Omega - \int_{\Gamma_{X_1=1}} (w_2 T_2 + w_3 T_3) \, \mathrm{d}\Gamma_{X_1=1} = 0, \quad \forall \boldsymbol{w} \in \mathcal{V} \tag{14}$$

where the first Piola-Kirchhoff stress tensor and the higher-order stress tensor in component form are:

$$P_{iJ} := \partial\Psi / \partial F_{iJ}, \tag{15a}$$
$$B_{iJK} := \partial\Psi / \partial F_{iJ,K}. \tag{15b}$$

We then assess stability of each solution by numerically checking the positive definiteness of the second variation as:

$$D^2\Pi[\boldsymbol{w}, \boldsymbol{w}] = \int_\Omega \left(w_{i,I} \frac{\partial^2 \Psi}{\partial F_{iI} \partial F_{jJ}} w_{j,J} + w_{i,I} \frac{\partial^2 \Psi}{\partial F_{iI} \partial F_{jJ,K}} w_{j,JK} + w_{i,IL} \frac{\partial^2 \Psi}{\partial F_{iI,L} \partial F_{jJ}} w_{j,J} + w_{i,IL} \frac{\partial^2 \Psi}{\partial F_{iI,L} \partial F_{jJ,K}} w_{j,JK} \right) \mathrm{d}\Omega > 0, \tag{16}$$

where, as in the one-dimensional case, we have explicitly retained the symmetric second and third terms of the integrand for clarity of the development. Note that, following standard variational arguments [9, 10], one can derive the strong form of the boundary value problem corresponding to the weak form (14) and (11) with (13) as:

$$-P_{iJ,J} + B_{iJK,JK} = 0 \quad \text{on } \Omega,$$

along with Neumann/higher-order Neumann conditions:

$$P_{i1} - B_{i11,1} - 2B_{i12,2} - 2B_{i13,3} = T_i,\ B_{i11} = 0,\ (i = 2, 3) \text{ on } X_1 = 1,$$
$$P_{iL} - 2(B_{iL1,1} + B_{iL2,2} + B_{iL3,3}) + B_{iLL,L} = 0,\ B_{iLL} = 0,\ (i = 1, 2, 3, \text{ no sum on } L) \text{ on } X_L = \{0, 1\}\ (L = 2, 3).$$

A more detailed treatment of these boundary conditions is found in the works of Toupin [9, 10].

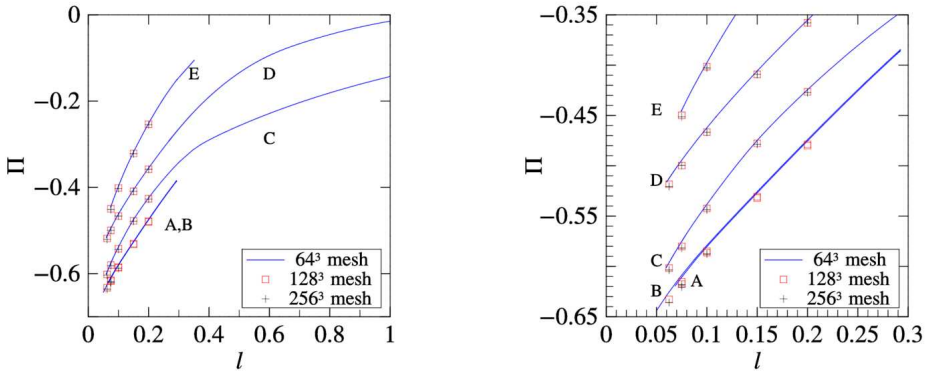

(a) (b)

Figure 5: Plots of total free energy Π v.s. length scale parameter l for branches A - E on (a) $(l, \Pi) \in [0, 1] \times [-0.70, 0]$ and (b) $(l, \Pi) \in [0, 0.3] \times [-0.65, -0.35]$. Note that branches A and B very nearly overlap in these plots. The blue curves were obtained by the branch-tracking technique on a 64^3 mesh. The data points represented by red squares were obtained by refining these solutions on a 128^3 mesh at selected values of l and those represented by black '+' signs were obtained by further refinement on a 256^3 mesh.

3.1 Numerics

We seek numerical solutions $\boldsymbol{u}^h \in \mathcal{S}^h \subset \mathcal{S}$ to a finite-dimensional counterpart of the weak form (14) defined for $\boldsymbol{w}^h \in \mathcal{V}^h \subset \mathcal{V}$, where:

$$\mathcal{S}^h = \{\boldsymbol{v}^h \in H^2(\Omega) | v_i^h = 0,\ v_{i,1}^h = 0 \text{ on } X_1 = 0, \text{ for } i = 1, 2, 3,\ v_1^h = 0,\ v_{1,1}^h = 0 \text{ on } X_1 = 1\}, \tag{18a}$$

$$\mathcal{V}^h = \{\boldsymbol{v}^h \in H^2(\Omega) | v_i^h = 0,\ v_{i,1}^h = 0 \text{ on } X_1 = 0, \text{ for } i = 1, 2, 3,\ v_1^h = 0,\ v_{1,1}^h = 0 \text{ on } X_1 = 1\}. \tag{18b}$$

The problem was solved using IGA. The finite-dimensional subspaces $\mathcal{S}^h$ and $\mathcal{V}^h$ were constructed using a second-order, C^1-continuous, B-spline basis defined in three dimensions on 64^3, 128^3, and 256^3 elements of uniform size, which enforce the Dirichlet/higher-order Dirichlet conditions *strongly*. IGA was previously employed to solve a range of boundary value problems with Toupin's theory of gradient elasticity at finite strain by Rudraraju et al. [7], with higher-order Dirichlet conditions applied *weakly*. Our code [8] is written in C. We use Mathematica 10 to symbolically produce elementwise residual/tangent evaluation routines, PETSc 3.7.4 for iterative linear/nonlinear solvers, SLEPc 3.7.3 for an eigenvalue problem solver, and mathgl 2.3.0 for plots. Specifically, MINRES with Jacobi preconditioner and a backtracking line search method with cubic-order approximation were chosen for iterative solvers. We used the double-precision floating-point format with absolute tolerance of 10^{-12} on the residual of the discretized, matrix-vector weak form. The floating point precision and residual tolerance were relaxed relative to the one-dimensional problem for numerical efficiency. In practice, the lower precision and less stringent tolerance were found to be adequate after using the more demanding thresholds in the one-dimensional case. The second variation (16) was discretized on the same B-spline basis, and the stability of each solution was assessed by extracting the lower end of the spectrum of eigenvalues of the corresponding symmetric Hessian matrices. For the eigenvalue problem, we used an absolute convergence error tolerance of 1×10^{-6}.

3.2 Solution branches and branch-tracking

We solved the boundary value problem on the 64^3 mesh, obtained five different branches, denoted by A - E, and computed the total free energy for these solutions over ranges of values of l; these computed values appear as solid curves in Fig. 5. At selected values of l, $l = 0.0625, 0.0750, 0.1000, 0.1500$, and/or 0.2000, solutions were refined on a 128^3 mesh and a 256^3 mesh, and are plotted in Fig. 5 by red squares and black '+' signs, respectively. Reparameterized strains, e_2 and e_3 (10a), obtained on the 128^3 mesh are plotted in Figs. 6 and 7 for each branch at selected values of l. In addition, values of e_2 and e_3 were computed at 33^3 uniformly spaced points in the body and were plotted on the $e_2 - e_3$ space in Fig. 8, superposed on the three-well diagram presented in Fig. 4a. The strain states corresponding to tetragonal variants 1, 2, and 3 appear in the orange, green, and brown wells, respectively. Fig. 9 shows three-variant plots that delineate sub-domains of the variants;

material points that lie in the interfaces between any two variants are colored in dark gray. Note that while branches A and B very nearly overlap in the $\Pi - l$ space of Fig. 5, the strains, microstructures and energy landscapes of these branches are actually vastly different as seen in Figs. 6-9.

The curves in Fig. 5 were obtained using a simple branch-tracking technique employed in the one-dimensional example in Sec. 2 with slight modification. For the purpose of demonstration, we aimed to obtain *moderately low-energy* microstructures for which tetragonal variants are well developed in the body for the free energy coefficient $B_5 = 180$ and in the vicinity of $l = 0.10$. Since such low-energy microstructures are under large strains, direct computation at $(B_5, l) = (180, 0.10)$ is not practical as we in general do not have *good* initial guesses with which we can obtain converged solutions in three dimensions. We thus first computed high-energy solutions under small strains at relatively large values of (B_5, l), and then employed branch-trackings in decreasing B_5- and l-directions down to $(B_5, l) = (180, 0.10)$, which would develop lower-energy microstructures under larger strains. Small-strain, high-energy solutions were obtained using either the homogeneous initial guess or random initial guesses of small magnitude. The former was used for branch E and the latter was used for branches A-D.

To eventually obtain solutions well resolved on the 64^3 mesh, we first computed the initial high-energy solutions on an 8^3 mesh or on a 16^3 mesh and successively refined them before branch-trackings. Finer initial meshes, say 32^3, would produce finer and more interesting microstructures at the end of the iterative process, but at the expense of greater computational complexity. Our goal being demonstration of the series of techniques, however, we do not pursue this approach here. For branch E, for instance, a solution was first computed with $(B_5, l) = (500, 0.54)$ on the 16^3 mesh using the homogeneous initial guess and successively refined onto the 64^3 mesh, which was then followed by branch-trackings as $(B_5, l) = (500, 0.54) \rightarrow (500, 0.15) \rightarrow (180, 0.15) \rightarrow (180, 0.10)$. Branch D, on the other hand, was first computed with $(B_5, l) = (500, 0.50)$ using a random initial guess of $|\boldsymbol{u}^h| \sim O(10^{-2})$ on the 8^3 mesh, successively refined onto the 64^3 mesh, and subject to branch-trackings as $(B_5, l) = (500, 0.54) \rightarrow (500, 0.27) \rightarrow (180, 0.27) \rightarrow (180, 0.10)$.

3.3 Numerical convergence

For added confidence that the branches obtained in this study are not numerical artifacts, we studied convergence of these solutions with mesh refinement; at selected values: $l = 0.0625$, 0.0750, 0.1000, 0.1500, and/or 0.2000, solutions were refined on a 128^3 mesh and a 256^3 mesh, and corresponding energy values were plotted in Fig. 5 as red squares and black '+' signs, respectively. Fig. 5a implies that, in general, solutions computed on the 64^3 mesh are energetically well converged and Fig. 5b indicates that solutions are better resolved for larger values of l, where the interface thickness is wider and microstructures are coarser. Refinement of branches A and B was more challenging especially for larger values of l, and refinement on the 256^3 mesh was only performed for $l \leq 0.1000$ for these branches. These branches also experience slightly larger deviation when refined as seen in Fig. 5b. We did not pursue these problems further as these branches are of little practical interest.

Fig.10, on the other hand, shows the distribution of the three variants making up the microstructure at $l = 0.0625$ for the 64^3, 128^3, and 256^3 meshes. Attention is drawn to the near complete convergence of solutions on the 64^3 mesh in the sense of microstructure.

3.4 Stability/metastability

The numerical study of the boundary value problem was followed by stability analysis, where positive definiteness of the Hessian derived from the second variation (16) was numerically checked for each branch. Table 1 shows the smallest eigenvalues of the Hessians for branches A - E on different refinement levels at selected values of l; positive values therefore imply stability/metastability. Branch A, though the smallest eigenvalue is negative at $l = 0.0750$ probably due to poor resolution, is most likely to be stable, which is consistent with that branch A is most likely to be the lowest-energy branch. Branch B, on the other hand, seems to gain stability somewhere between $l = 0.1000$ and $l = 0.1500$. Portions of branch C and branch D would also be good candidates for metastable portions of branches, considering the convergence behavior of the eigenvalues with mesh refinement. The stability/metastability behavior of the branches with decreasing l points to the existence of as yet undiscovered branches at increasingly finer microstructure. Their resolution is only limited by the numerical expense of ever finer meshes.

3.5 Parametric dependence of twin microstructures

One can make several important observations for the solutions obtained in this section. As was also observed in one dimension, the interfaces between tetragonal variants, which are represented by the dark gray regions in Fig. 9, become sharper as the length scale parameter l decreases, the state of much of the material descending into the energy wells as indicated in Figs. 8. These plots also highlight how a richer microstructure develops at lower values of l, with more material points being localized to those wells that are sparsely populated at higher l. Fig. 9 also suggests that the interface thickness is proportional to l and that, at a fixed value of l, the thickness

Branch	mesh	$l = 0.0625$	$l = 0.0750$	$l = 0.1000$	$l = 0.1500$	$l = 0.2000$
E	64^3		-0.088755	-0.065765	-0.040403	-0.027748
	128^3		-0.020364	-0.013910	-0.007705	-0.004932
	256^3		-0.003886	-0.002482	-0.001261	-0.009806
D	64^3	-0.000301	-0.000285	-0.000284	-0.000283	-0.000206
	128^3	-0.000041	-0.000038	-0.000038	-0.000037	-0.000027
	256^3	-0.000005	-0.000005	-0.000005	-0.000005	-0.011602
C	64^3	-0.046564	-0.022921	-0.000227	-0.000264	-0.000169
	128^3	-0.006671	-0.003216	-0.000030	-0.000034	-0.000023
	256^3	-0.000861	-0.000408	-0.000004	-0.000004	-0.006915
B	64^3	-0.007714	-0.008696	-0.008139	0.000352	0.000350
	128^3	-0.001112	-0.001184	-0.001133	0.000046	0.000046
	256^3	-0.000143	-0.000152	-0.000147		
A	64^3		-0.003220	0.000313	0.000352	0.000350
	128^3		-0.000522	0.000041	0.000046	0.000046
	256^3		-0.000070			

Table 1: Smallest eigenvalues of the Hessians corresponding to the discretized counterpart of the second variation (16) for branches A - E at different refinement levels for selected values of l. Positive values indicate stable/metastable solutions.

is virtually the same over different branches – an observation that can also be made for the one-dimensional problem in Sec. 2 from Fig. 3. One can further infer from Figs. 5 and 9 that, regardless of stability, the equilibrium solutions achieving relatively low total free energy form via tetragonal variants with twin interfaces. This is as shown for the limiting case of $l = 0$ in Fig. 4b according to the pure energy minimization argument. Fig. 11, for instance, shows the twin-structures observed in branches B and D at $l = 0.0625$; Fig. 4b is repeated here to ease comparison.

4 Conclusion and future works

We have considered martensitic phase transformations in three dimensions that are modeled by a free energy density function that is non-convex in strain space, and is regularized by Toupin's theory of gradient elasticity at finite strain. There exist three minima in the non-convex free energy density in strain space, corresponding to three, symmetrically equivalent, tetragonal, martensitic variants. The single maximum represents the cubic, austenite. Our primary interest was to establish numerical procedures to obtain solution branches corresponding to the extrema/saddle points of the total free energy, and to assess their stability. To this end, we have employed a simple branch-tracking technique to continuously follow a solution branch along the strain gradient length-scale parameter starting from the first solution computed using either a random initial guess or the homogeneous initial guess. The stability of each solution was then investigated in terms of the positive definiteness, or lack thereof, of the second variation of the total free energy. Each solution branch corresponds to a distinct twinned microstructure for the same boundary value problem. The phase interfaces between energetically stable tetragonal variants in a microstructure become sharper as the length scale parameter decreases. The microstructures of certain branches themselves become richer with variants missing at higher values of l emerging at lower l. To our knowledge this is the first work that comprehensively studies branching of solutions and observed twin structures in three-dimensional diffuse-interface problems based on a non-convex density function regularized by strain gradient terms.

This work forms a foundation to study shape-memory alloys under loading, where different microstructures are experimentally observed for the same set of boundary conditions. A proper investigation of that class of problems also requires the incorporation of elastodynamics, in which case, the variations from initial conditions lead to different solution branches and therefore different microstructures for the same set of boundary conditions. A more direct comparison with experiments also needs a treatment of plasticity coupled with twinning as modelled here. This work also provides a basis to study the homogenized response of a material exhibiting the microstructures corresponding to different solution branches. From such a study it may be possible to develop reduced order, effective constitutive models that also incorporate the evolution of martensitic microstructures.

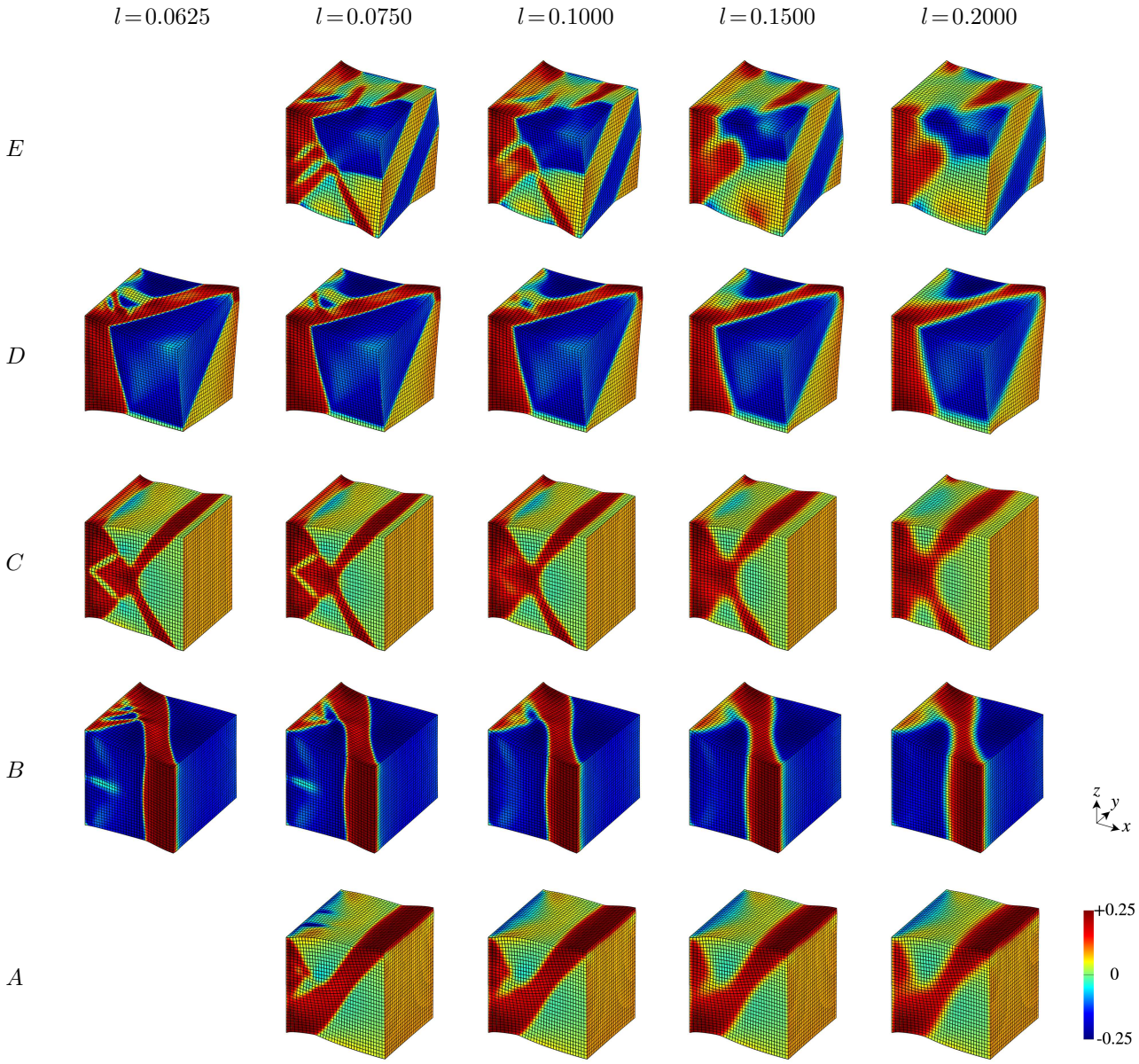

Figure 6: Field values of e_2 for branches A - E on deformed configurations for selected values of l. Solutions on the 128^3 mesh have been overlaid with a 32^3 plotting mesh.

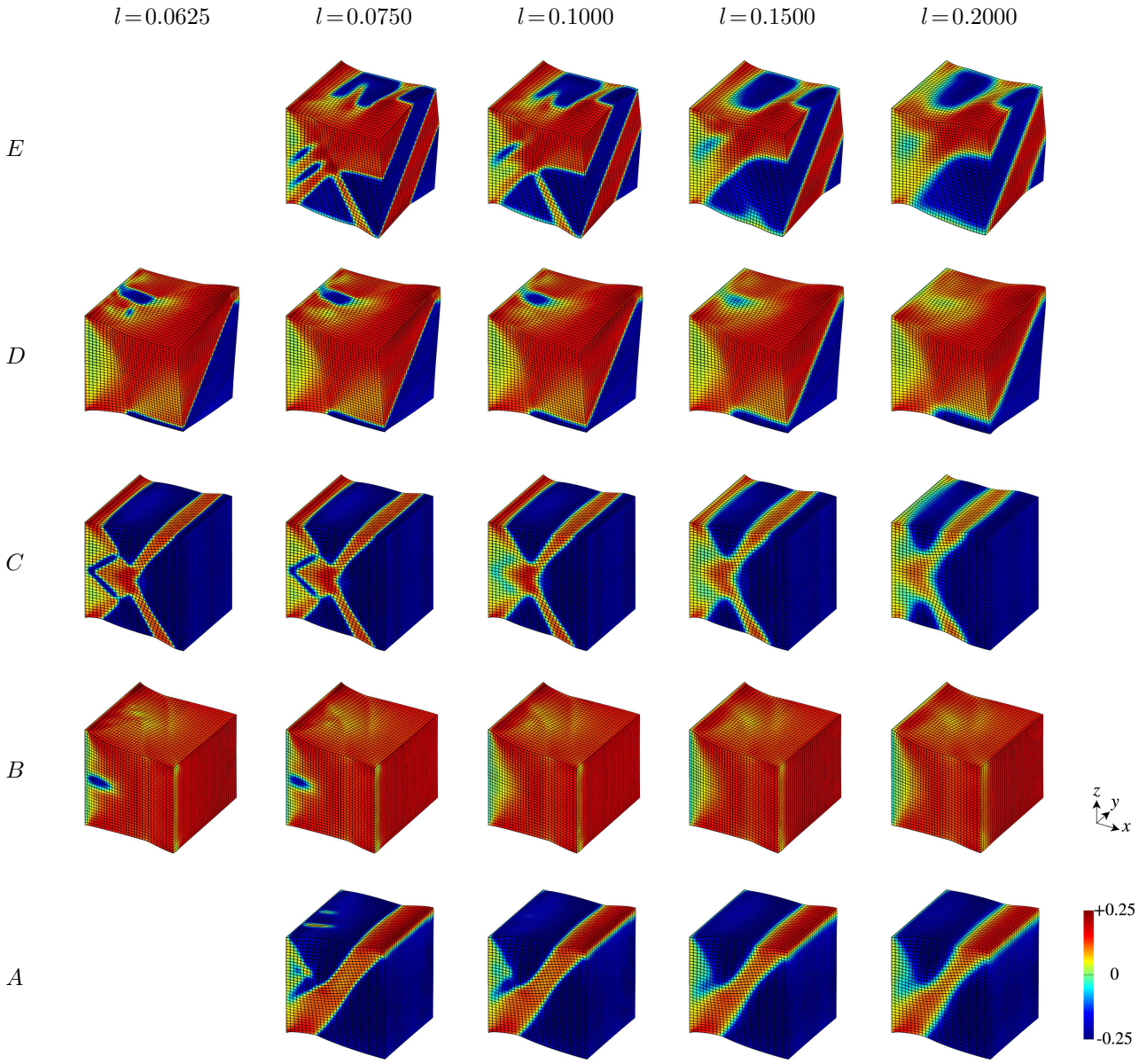

Figure 7: Field values of e_3 for branches A - E on deformed configurations for selected values of l. Solutions on the 128^3 mesh have been overlaid with a 32^3 plotting mesh.

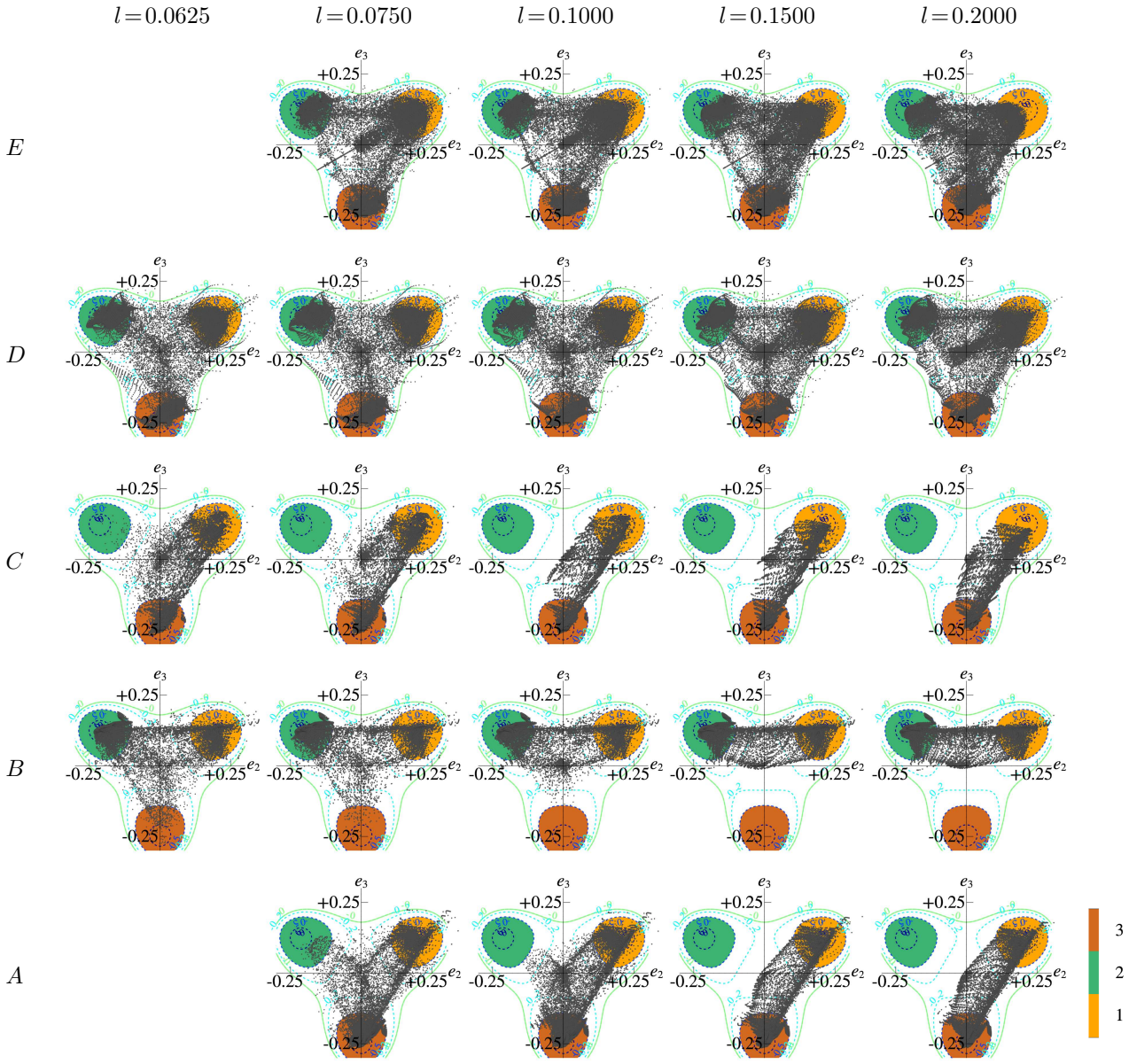

Figure 8: Contours of (e_2, e_3) for branches A - E computed from the solutions on the 128^3 mesh at 33^3 uniformly spaced points. Selected values of l are indicated. The three-well contour diagram, Fig. 4a, is also shown, underlying each plot as an indicator of the formation of tetragonal variants.

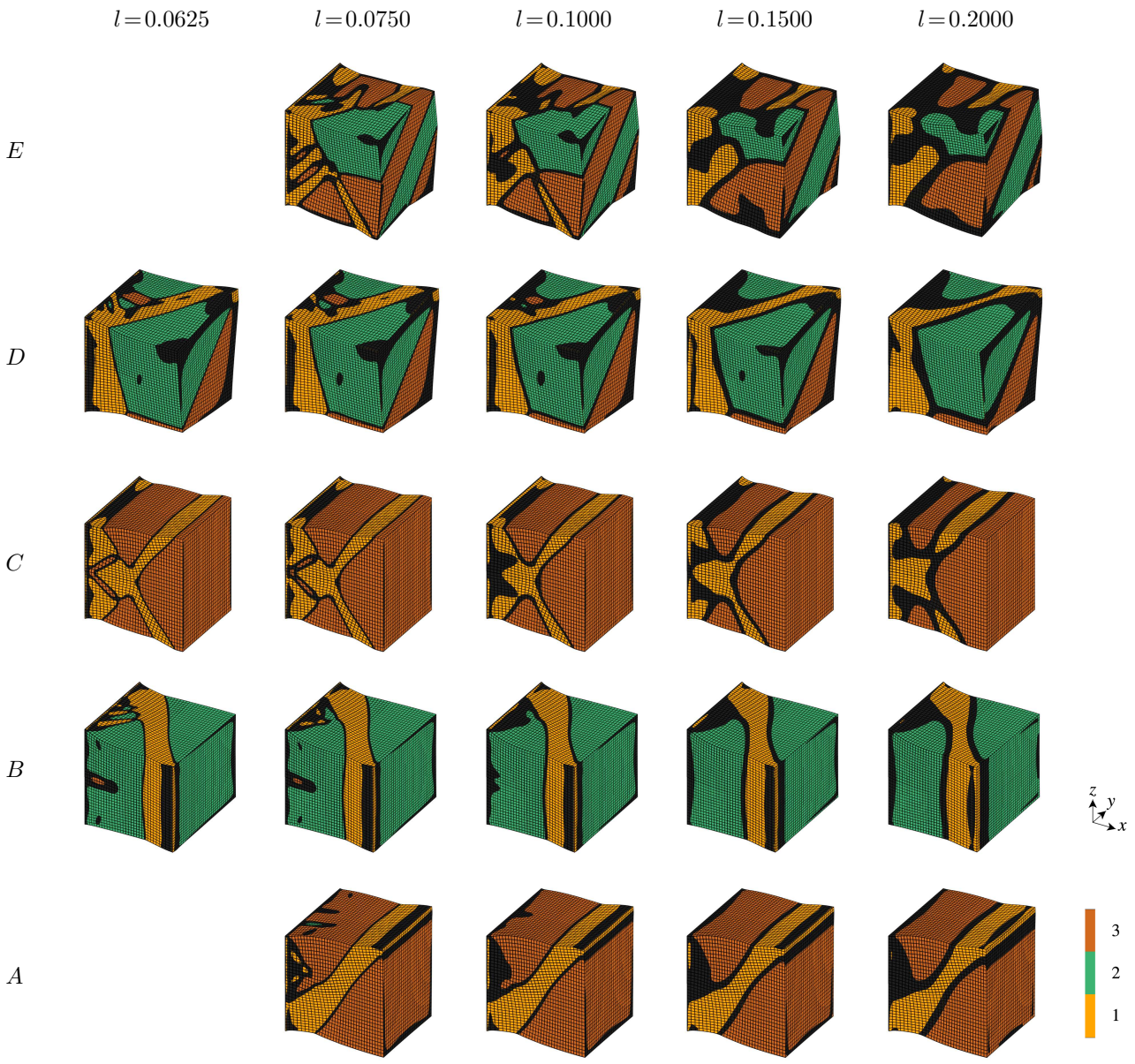

Figure 9: Distribution of the three tetragonal variants for branches A - E on deformed configurations for selected values of l. Solutions on the 128^3 mesh have been overlaid with a 32^3-plotting mesh. The three tetragonal variants are indicated by different colors; see Fig. 4a.

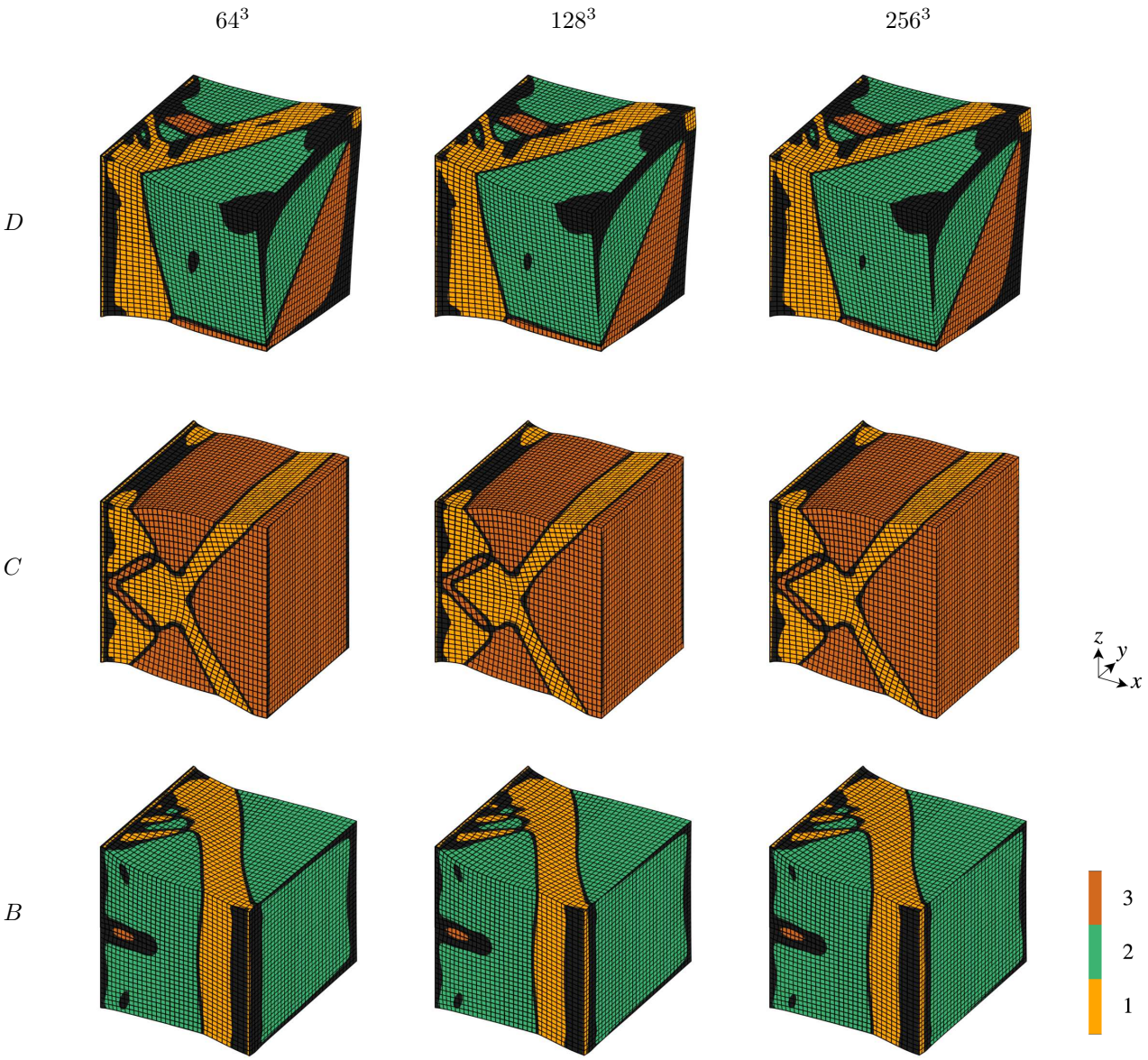

Figure 10: Convergence study of the distribution of tetragonal variants in the microstructure for branches B, C, and D. Solutions were computed at $l = 0.0625$ on the 64^3, 128^3, and 256^3 meshes. All plots were overlaid with a 32^3 plotting mesh.

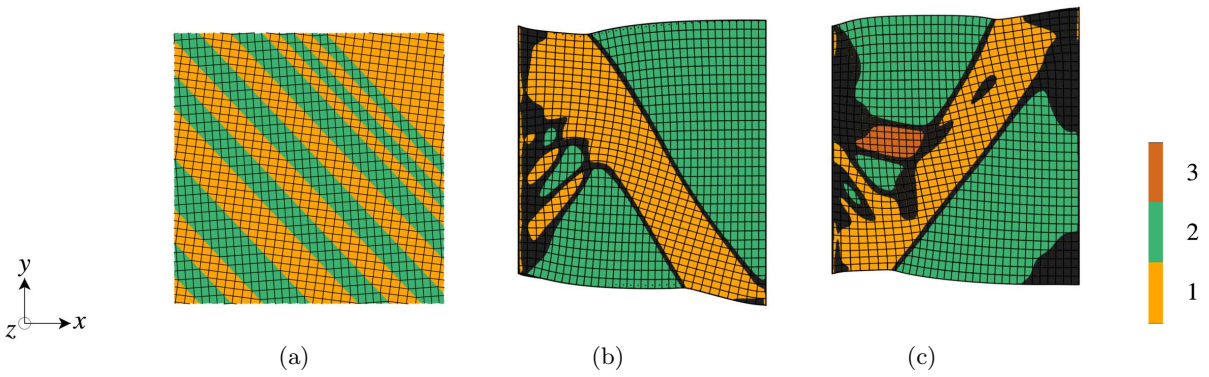

(a) (b) (c)

Figure 11: (a) One typical solution expected from the pure energy minimization argument for $l = 0$, showing twinning between tetragonal variants 1 and 2 (reproduced from Fig. 4b). Top-views of the microstructures with twinning for (b) branch B and (c) branch D obtained from the boundary value problem at $l = 0.0625$.

Acknowledgments

The numerical formulation and computations have been carried out as part of research supported by the U.S. Department of Energy, Office of Basic Energy Sciences, Division of Materials Sciences and Engineering under Award #de-sc0008637 that funds the PRedictive Integrated Structural Materials Science (PRISMS) Center at University of Michigan. This work used the Extreme Science and Engineering Discovery Environment (XSEDE), which is supported by National Science Foundation grant number ACI-1053575. We used XSEDE resources [11] through the Campus Champions program. The numerical computations in three dimensions presented here also made intensive use of resources of the National Energy Research Scientific Computing Center, a DOE Office of Science User Facility supported by the Office of Science of the U.S. Department of Energy under Contract No. DE-AC02-05CH11231. Finally, this research was supported in part through computational resources and services provided by Advanced Research Computing at the University of Michigan, Ann Arbor.

References

[1] J. M. Ball and R. D. James. Fine phase mixtures as minimizers of energy. *Archive for Rational Mechanics and Analysis*, 100:13–52, 1987.

[2] Jack Carr, Morton E. Gurtin, and Marshall Slemrod. Structured phase transitions on a finite interval. *Archive for Rational Mechanics and Analysis*, 86:317–351, 1984.

[3] Michel Chipot and David Kinderlehrer. Equilibrium configurations of crystals. *Archive for Rational Mechanics and Analysis*, 103:237–277, 1988.

[4] J. Austin Cottrell, Thomas J. R. Hughes, and Yuri Bazilevs. *Isogeometric Analysis*. John Wiley & Sons, Ltd, 2009.

[5] Timothy J Healey and Ulrich Miller. Two-phase equilibria in the anti-plane shear of an elastic solid with interfacial effects via global bifurcation. *Proceedings of the Royal Society of London A: Mathematical, Physical and Engineering Sciences*, 463:1117–1134, 2007.

[6] Eric Polizzi. Density-matrix-based algorithm for solving eigenvalue problems. *Phys. Rev. B*, 79:115112, Mar 2009.

[7] S. Rudraraju, A. Van der Ven, and K. Garikipati. Three-dimensional isogeometric solutions to general boundary value problems of Toupin's gradient elasticity theory at finite strains. *Computer Methods in Applied Mechanics and Engineering*, 278:705 – 728, 2014.

[8] K. Sagiyama. `IGAP4GradElast`: An isogeometric analysis program for gradient elasticity written in `C` and aided by `Mathematica`. . `https://github.com/mechanoChem/IGAP4GradElast`, 2017.

[9] R.A. Toupin. Elastic materials with couple-stress. *Archive for Rational Mechanics and Analysis*, 11:385–414, 1962.

[10] R.A. Toupin. Theories of elasticity with couple-stress. *Archive for Rational Mechanics and Analysis*, 17:85–112, 1964.

[11] John Towns, Timothy Cockerill, Maytal Dahan, Ian Foster, Kelly Gaither, Andrew Grimshaw, Victor Hazlewood, Scott Lathrop, Dave Lifka, Gregory D. Peterson, Ralph Roskies, J. Ray Scott, and Nancy Wilkins-Diehr. Xsede: Accelerating scientific discovery. *Computing in Science & Engineering*, 16(5):62–74, 2014.

[12] Lev Truskinovsky and Giovanni Zanzotto. Finite-scale microstructures and metastability in one-dimensional elasticity. *Meccanica*, 30:577–589, 1995.

[13] Lev Truskinovsky and Giovanni Zanzotto. Ericksen's bar revisited : Energy wiggles. *Journal of the Mechanics and Physics of Solids*, 44:1371 – 1408, 1996.

[14] A. Vainchtein, T. Healey, P. Rosakis, and L. Truskinovsky. The role of the spinodal region in one-dimensional martensitic phase transitions. *Physica D: Nonlinear Phenomena*, 115:29 – 48, 1998.

[15] Anna Vainchtein, Timothy J. Healey, and Phoebus Rosakis. Bifurcation and metastability in a new one-dimensional model for martensitic phase transitions. *Computer Methods in Applied Mechanics and Engineering*, 170:407 – 421, 1999.